Supplementary Information to: Feedback Between Climate and Geodynamics Leads to Bistability in Conceptual Models

Kaspar Görg, Julius Eberhard and Georg Feulner

July 14, 2026

S1 Full model description

The model consists of three modules, representing the climate system, the carbon cycle, and geodynamics (see figure 1). The climate module is an equilibrium global energy balance model with a temperature-dependent albedo to represent the ice-albedo feedback. The carbon cycle model comprises three reservoirs (one combined reservoir for atmosphere and ocean, one for the ocean crust, and one for the mantle). Fluxes between these reservoirs arise from weathering, volcanic outgassing, and crustal subduction. The geodynamics model includes a weatherability variable representing the amount of weathering that occurs under given climatic conditions. In the main model, weatherability is kept fixed, while in an extended model version, we let it vary dynamically. Furthermore, the geodynamics module includes a parametrization of the plate velocity depending on sediment flux.

The climate and the carbon cycle module are coupled via the dependence of the outgoing long-wave radiation on the partial pressure of CO_2, p_{CO_2}, and the temperature and p_{CO_2} dependence of weathering, establishing a weathering thermostat [1]. The geodynamics module is coupled to the carbon module due to the dependence of outgassing, subduction, and seafloor weathering on plate velocity. Finally, the geodynamics module is coupled to the climate module via the dependence of plate velocity on erosion, which in turn is influenced by temperature.

In contrast to the main paper, we give variables in SI units. Variables V that are given in units of their present-day values V_0 will be denoted with an asterisk V^* in the following.

All model variables are listed in tables 1 (climate model), 3 (carbon cycle model), and 5 (geodynamics model), and all parameter values are given in tables 2 (climate model), 4 (carbon cycle model), and 6 (geodynamics model).

S1.1 Climate model

We use a global energy balance model, in which the difference between absorbed short-wave radiation (ASR) and outgoing long-wave radiation (OLR) determines the rate of global temperature change dT/dt depending on the climate system's heat capacity C:

$$C\frac{dT}{dt} = \mathrm{ASR}(T) - \mathrm{OLR}(T). \tag{1}$$

Since geological processes generally evolve on much longer timescales than the climate system, we assume that climate is always in equilibrium, i.e. the heat capacity vanishes: $C = 0$. This turns Eq. 1 from a prognostic into a diagnostic equation, allowing to determine the equilibrium temperature from $p_{\mathrm{CO_2}}$ at each time step.

To parametrize the outgoing long-wave radiation, we use the formulation by Williams and Kasting [2], which is applicable in a $p_{\mathrm{CO_2}}$ range from $1\,\mathrm{Pa}$ to $1 \times 10^6\,\mathrm{Pa}$:

$$\begin{aligned}\mathrm{OLR} =&9.468980 - 7.714727 \times 10^{-5}\phi - 2.794778T - 3.244753\\ &\times 10^{-3}\phi T - 3.547406 \times 10^{-4}\phi^2 + 2.212108 \times 10^{-2}T^2\\ &+ 2.229142 \times 10^{-3}\phi^2 T + 3.088497 \times 10^{-5}\phi T^2\\ &- 2.789815 \times 10^{-5}\phi^2 T^2 - 3.442973 \times 10^{-3}\phi^3 - 3.361939\\ &\times 10^{-5}T^3 + 9.173169 \times 10^{-3}\phi^3 T - 7.775195\\ &\times 10^{-5}\phi^3 T^2 - 1.679112 \times 10^{-7}\phi T^3 + 6.590999\\ &\times 10^{-8}\phi^2 T^3 + 1.528125 \times 10^{-7}\phi^3 T^3 - 3.367567 \times 10^{-2}\phi^4\\ &- 1.631909 \times 10^{-4}\phi^4 T + 3.663871 \times 10^{-6}\phi^4 T^2\\ &- 9.255646 \times 10^{-9}\phi^4 T^3,\end{aligned} \tag{2}$$

with $\phi = \ln\dfrac{p_{\mathrm{CO_2}}}{33\,\mathrm{Pa}}$ [2]. We modify the OLR parametrization by adding a constant value to let the model be in steady state for pre-industrial conditions.

The absorbed solar radiation ASR is determined from the solar irradiance S and from Earth's albedo α:

$$\mathrm{ASR} = \frac{S}{4}(1-\alpha). \tag{3}$$

Due to the sun's evolution as a main sequence star, its luminosity changes over geological time. The standard approximation is given by [3]

$$S(t) = \left[1 + \frac{2}{5}\left(1 - t/t_{\odot}\right)\right]^{-1} S_0, \tag{4}$$

where S_0 is the present-day solar irradiance and $t_{\odot}$ is the age of the sun. Using this approximation, insolation at the start of the Marinoan glaciation was approximately 6 % lower than today and 13 % lower at the start of the Boring Billion.

In order to be able to reproduce the Snowball Earth state, the model must incorporate the ice-albedo feedback. Therefore, the albedo must be parametrized as a function of temperature, representing albedo values from Snowball to ice-free state. We transition between high and low albedo using a sigmoid function after North and Kim [4]:

$$\alpha(T) = \alpha_{\mathrm{ice}} + \frac{1}{2}(\alpha_{\mathrm{no-ice}} - \alpha_{\mathrm{ice}})(1 + \tanh \gamma_{\mathrm{albedo}}(T - T_{\mathrm{ref}})). \tag{5}$$

The values for the high and low albedo α_{ice} and $\alpha_{\mathrm{no-ice}}$ are taken in accordance with the parametrizations by Mills et al. [5] and Abbot et al. [6], the transition point T_{ref} and width γ_{albedo} are tuned to give realistic glaciation (271 K, ignoring stable Hadley states [7]) and deglaciation (265 K [8]) temperatures. This approach is therefore likely to produce realistic results while keeping the complexity of the underlying assumptions to a minimum.

S1.2 Carbon cycle model

The carbon cycle model has been adapted from the work of Foley [9]. There are three carbon reservoirs: The plate C_{p}, the mantle C_{m} and a combined atmosphere and ocean reservoir $C_{\mathrm{a+o}}$. Carbon is removed from the atmosphere and ocean reservoir and added to the plate reservoir via weathering F_{w}, which has contributions from continent weathering F_{cw} and seafloor weathering F_{sfw}. Since for every two molecules of CO_2 absorbed in the weathering reaction, one is eventually returned to the atmosphere, the continent weathering flux is divided by 2. Subduction of carbon F_{sub} results in some of it being degassed into the atmosphere fF_{sub} and some being recycled into the mantle $(1-f)F_{\mathrm{sub}}$. Degassing from the mantle into the atmosphere F_{degas} closes the system.

$$\frac{dC_{\mathrm{p}}}{dt} = \frac{F_{\mathrm{cw}}(C_{\mathrm{o+a}})}{2} + F_{\mathrm{sfw}}(C_{\mathrm{o+a}}) - F_{\mathrm{sub}}(C_{\mathrm{p}}) \tag{6}$$

$$\frac{dC_{\mathrm{m}}}{dt} = (1-f)F_{\mathrm{sub}}(C_{\mathrm{p}}) - F_{\mathrm{degas}}(C_{\mathrm{m}}) \tag{7}$$

$$\frac{dC_{\mathrm{a+o}}}{dt} = fF_{\mathrm{sub}}(C_{\mathrm{p}}) + F_{\mathrm{degas}}(C_{\mathrm{m}}) - \frac{F_{\mathrm{cw}}(C_{\mathrm{o+a}})}{2} - F_{\mathrm{sfw}}(C_{\mathrm{o+a}}) \tag{8}$$

We tune the total amount of carbon to let present-day outgassing match present-day weathering (see section S2).

We often use a shorthand notation for the total rate of weathering,

$$F_{\mathrm{w}} = \frac{F_{\mathrm{cw}}}{2} + F_{\mathrm{sfw}}, \tag{9}$$

and the total rate of outgassing into the atmosphere,

$$F_{\mathrm{out}} = F_{\mathrm{degas}} + fF_{\mathrm{sub}}. \tag{10}$$

S1.2.1 Degassing and Subduction

The formulations of the degassing and subduction flux are also adapted from Foley [9]:

$$F_{\mathrm{degas}} = f_{\mathrm{d}} \frac{C_{\mathrm{m}}}{V_{\mathrm{m}}} 2Ld_{\mathrm{melt}} v_{\mathrm{p}} \tag{11}$$

$$F_{\mathrm{sub}} = \frac{C_{\mathrm{p}} L}{A_{\mathrm{p}}} v_{\mathrm{p}} \tag{12}$$

Here, the degassing ratio f_{d} is tuned to match the present-day degassing flux [9]. The length of ridges and the length of trenches are assumed to be identical [9].

To incorporate a carbon degassing flux independent of plate velocity, e.g., due to plume volcanism, we modify Eq. 11:

$$F_{\mathrm{degas}} = \zeta f_{\mathrm{d}} \frac{C_{\mathrm{m}}}{V_{\mathrm{m}}} 2Ld_{\mathrm{melt}} v_{\mathrm{p}} + (1-\zeta)HC_{\mathrm{m}}. \tag{13}$$

Here, ζ is the ratio of plate-velocity dependent degassing to total mantle degassing, and H is a constant to ensure that the total outgassing flux is independent of ζ at pre-industrial conditions. In the main model, we use the simplified case $\zeta = 1$. In the extendend model version, we use $\zeta = 0.5$. Also see section S4 for a derivation of the ζ parameter and a detailed discussion on the influence of ζ on the climate of the slow plate velocity state.

S1.2.2 Continent weathering

We determine the continent weathering rate as described by Krissansen-Totton and Catling [10]:

$$F_{\mathrm{cw}} = F_{\mathrm{cw},0} W (\mathrm{pCO}_2^*)^{a_{\mathrm{cw}}} \exp\left(\frac{T - T_0}{T_{\mathrm{cw}}}\right). \tag{14}$$

Here, the present-day weathering flux $F_{\mathrm{cw},0}$ is scaled by a weatherability factor W, a p_{CO_2} and a temperature dependence. The direct dependence on temperature and the indirect dependence on temperature via precipitation are subsumed in one exponential function [10]. The e-folding temperature T_{cw} indicates by how much temperature has to increase to let weathering increase by a factor of e. Estimates of the e-folding temperature T_{cw} usually range from 10 [11, 12] to 20 K [13]; however, Krissansen-Totton and Catling give a much higher value of 34 K [10]. We use a value of $T_{\mathrm{cw}} = 10\,\mathrm{K}$ and show that our results do not depend sensitively on this choice.

Furthermore, to account for the suppressed hydrological cycle during a Snowball Earth event, the weathering flux is set to zero when global temperatures T fall below the Snowball transition temperature T_{ref}, similarly to Mills et al. [5], who reduce the weathering flux to 1 % of its original value during a Snowball event.

S1.2.3 Seafloor weathering

We use a standard expression for the seafloor weathering flux [10, 14]:

$$F_{\mathrm{sfw}} = k_{\mathrm{diss}} v_{\mathrm{p}}^* \exp\left(\frac{-E_{\mathrm{bas}}}{RT_{\mathrm{p}}}\right) \left([H^+]^*\right)^{\gamma_{\mathrm{sfw}}}. \tag{15}$$

The seafloor weathering rate F_{sfw} scales linearly with plate velocity v_{p}, exponentially with pore temperature T_{p} and via a power law with hydrogen molarity $[H^+]$.

Pore temperature T_p is linearly related to the surface temperature T [10]:

$$T_\mathrm{p} = c_{\mathrm{deep-water}} T + b_{\mathrm{deep-water}} + b_{\mathrm{pore}}. \tag{16}$$

This equation computes the deep water temperature and converts it into pore temperature by adding a heating constant due to the circulation of the water through warm crust, $b_{\mathrm{pore}} = 9\,\mathrm{K}$. Changes in the heating rate due to changing sediment thickness [15] or tectonic activity are neglected.

We also assume that the minimum deep-water temperature is $4\,^\circ\mathrm{C}$, leading to a minimum pore temperature of $T_\mathrm{p} = 286\,\mathrm{K}$, similarly to Chambers [16].

The dependence of hydrogen molarity on $p_{\mathrm{CO_2}}$ will be covered in section S1.2.5. Finally, the dissolution constant k_{diss} is tuned to let the seafloor weathering rate match the present-day rate under present-day conditions [14].

S1.2.4 Estimation of pCO2

We need to calculate the partial pressure of carbon dioxide $p_{\mathrm{CO_2}}$ from the total amount of carbon in the combined atmosphere-ocean reservoir $C_{\mathrm{o+a}}$ because the temperature in the climate model and the weathering reactions are given as functions of $p_{\mathrm{CO_2}}$, and not of $C_{\mathrm{o+a}}$ directly.

To relate $p_{\mathrm{CO_2}}$ to $C_{\mathrm{o+a}}$, we first have to find relationships between $p_{\mathrm{CO_2}}$ and the individual reservoirs C_a (atmosphere) and C_o (ocean). The amount of carbon dioxide in the atmosphere C_a can be related to $p_{\mathrm{CO_2}}$ as follows. Atmospheric pressure at sea level p is given by

$$p = \frac{g M_\mathrm{A}}{A_{\mathrm{Earth}}}, \tag{17}$$

where g is the gravitational acceleration, M_A is the mass of the atmosphere, and A_{Earth} is the surface area of the Earth. The partial pressure of CO_2 is then obtained by multiplying by the molar concentration of CO_2, i.e. the number of moles in the atmosphere C_a divided by the total number of moles in the atmosphere N, resulting in

$$p_{\mathrm{CO_2}} = \frac{C_\mathrm{a}}{N} \frac{g M_\mathrm{A}}{A_{\mathrm{Earth}}} = C_\mathrm{a} \frac{\mu_{\mathrm{atm}} g}{A_{\mathrm{Earth}}}. \tag{18}$$

In the second step, M_A/N has been replaced by the average molar mass of the atmosphere, μ_{atm}. A similar equation is used by Foley [9] or Franck et al. [17]; however, instead of the average atmospheric molar mass μ_{atm}, they use the molar mass of CO_2. This results in an underestimation of the size of the atmospheric reservoir by a factor of 1.5 for a present-day atmospheric composition, since $\mu_{CO_2} \approx 1.5\mu_{\text{atm}}$. However, this error does not significantly affect the model behaviour, since the oceanic reservoir dominates over the atmospheric reservoir in terms of size.

We relate the amount of carbon in the oceans C_o to p_{CO_2} using the formulation given by Franck et al. [17]:

$$C_\text{o} = \alpha_{H_2O} K_0 V_{H_2O} \left(\frac{1}{\gamma_{H_2CO_3}} + \frac{K_1}{[H^+]\gamma_{HCO_3{}^-}} + \frac{K_1 K_2}{[H^+]^2 \gamma_{CO_3{}^{2-}}} \right) p_{CO_2} \tag{19}$$

Here, V_{H_2O} is the volume of the oceans, $[H^+]$ is the hydrogen molarity, and α_{H_2O}, γ_i and K_i are coefficients.

By combining equations 18 and 19, p_{CO_2} can be related directly to the combined reservoir $C_{\text{o+a}}$:

$$C_{\text{o+a}} = \underbrace{p_{CO_2} \alpha_{H_2O} K_0 V_{H_2O} \left(\frac{1}{\gamma_{H_2CO_3}} + \frac{K_1}{[H^+]\gamma_{HCO_3{}^-}} + \frac{K_1 K_2}{[H^+]^2 \gamma_{CO_3{}^{2-}}} \right)}_{C_\text{o}} + \underbrace{p_{CO_2} \frac{A_{\text{Earth}}}{g \mu_{CO_2}}}_{C_\text{a}} . \tag{20}$$

S1.2.5 Estimation of hydrogen molarity

Finally, the dependence of hydrogen molarity $[H^+]$ on p_{CO_2} needs to be taken into account. We use a linear relation between pH and $\log(p_{CO_2})$, which has been obtained from a more comprehensive ocean chemistry model [15]:

$$\log_{10} p_{CO_2} = -c_{\text{pH}} \text{pH} + b_{\text{pH}}. \tag{21}$$

Using the definition of pH,

$$\text{pH} = -\log_{10}[H^+], \tag{22}$$

this yields the p_{CO_2} dependence of $[H^+]$ [14, 15]

$$[H^+] = 10^{-b_{\text{pH}}/c_{\text{pH}}} \left(p_{CO_2}{}^* \right)^{1/c_{\text{pH}}} . \tag{23}$$

Note that our parametrization differs from the equation given by Krissansen-Totton et al. (their equation S23) in the prefactor $10^{-b_{\text{pH}}/c_{\text{pH}}}$, where they give $10^{-b_{\text{pH}}}$ [15].

Problematically, the dependence of p_{CO_2} on pH obtained in this way is so weak that combined with equation 20 it leads to a reduction in C_{o+a} with increasing p_{CO_2}. However, Krissansen-Totton et al. note that "the gradients of individual model realizations are typically steeper than the best fit straight line" [15]. We therefore adjust the coefficients c_{pH} and b_{pH} such that the straight line approximation follows roughly the mode of their results. Additionally, we set the maximum pH to 8.3, which corresponds to the minimum p_{CO_2} in the data, to improve numerical stability at low p_{CO_2}. This results in a well-defined relation between p_{CO_2} and C_{o+a}, which also aligns well with the parametrization used by Mills et al. [5].

S1.3 Geodynamics

We incorporate two main geodynamical mechanisms into the model: We parametrize plate velocity as a function of sediment flux and we let weatherability evolve according to mountain uplift – which we scale with plate velocity – and erosion.

S1.3.1 Plate velocity parametrization

As described in the main text, we use a sigmoid function to parametrize plate velocity as a function of sediment flux:

$$v_p = v_{min} + \frac{1}{2}(v_{max} - v_{min})(\tanh s_p(F_S - F_{S,ref}) + 1). \tag{24}$$

We let the maximum plate velocity $v_{p,max}$ equal the present-day plate velocity $v_{p,0}$ and set the minimum plate velocity to $0.2\,v_{max}$, corresponding to a change by almost one order of magnitude.

We estimate the reference flux $F_{S,ref}$, at which plate velocity transitions between the low and high regime, from the sediment thickness necessary to affect subduction zones. We assume that the transition occurs between a sediment thickness of 500 m and 1500 m, which is consistent with observations of shear stresses in subduction zones [18, 19] as well as numerical geodynamic models [20]. To convert sediment thickness h_s into a global flux of subducted sediments, we multiply with plate velocity v_p, the length of subduction zones L, sediment density $\rho_s = 2600\,\mathrm{kg\,m^{-3}}$, and the ratio of subducted (versus accreted) sediments f_s. For the sediment-starved case, we use $v_p = v_{p,min}$ and $f_s = 0.6$; for the lubricated case $v_p = v_{p,max}$ and $f_s = 0.2$ [21]. We then divide by the ratio of sediments that are deposited in trenches, which we estimate by the length of trenches L divided by the total continental coast length $L_{\mathrm{shore}} \approx 700\,000\,\mathrm{km}$ [22] to obtain the global sediment flux to the oceans F_{s}. This results in a sediment flux of $F_{\mathrm{s}} \approx 5\,\mathrm{Gt\,yr^{-1}}$ for the sediment-starved case and $fs \approx 14\,\mathrm{Gt\,yr^{-1}}$ for the well-lubricated case. The intermediate value of $F_{\mathrm{s}} \approx 10\,\mathrm{Gt\,yr^{-1}}$ corresponds to approximately 2/3 of the average Holocene sediment flux of $16\,\mathrm{Gt\,yr^{-1}}$[23]. Therefore we set the transition point to $F_{\mathrm{s,ref}} = 2/3\,F_{\mathrm{s,0}}$. For the steepness of the transition s_{p} we assume that at a sediment flux of $F_{\mathrm{s}} = 3/2\,F_{\mathrm{cw,ref}}$, plate velocities should already be approximately at the maximum plate velocity, which is the case if the argument of the tanh-function is approximately 2, since $\tanh(2) \approx 96\,\%$. This assumption leads to a choice of

$$s_{\mathrm{p}} = \frac{4}{F_{\mathrm{s,ref}}}. \tag{25}$$

S1.3.2 Dynamic evolution of weatherability

In the main model, we treat weatherability W as an external parameter. In the extended model version, we let W evolve dynamically to take into account the effect of tectonic activity on orogenesis and therefore weatherability.

Since most weathering occurs in mountains [24], we treat weatherability as a measure of the mass of all rocks in mountains. Therefore, weatherability is reduced by erosion E, and increased by mountain uplift. Analogously to Höning and Spohn, we assume that mountain production scales linearly with plate velocity v_{p} [25]. For simplicity, we neglect the direct dependence of volcanism on sediment subduction [26]. This leads to the following equation

$$\frac{dW^*}{dt} = \xi_1 v_{\mathrm{p}}^* - \xi_2 E^*(W), \tag{26}$$

with constants ξ_i, where erosion E^* scales linearly with W^* (see equation 27).

A rough estimate of ξ_2 can be obtained by relating the 50 % contribution to present-day global erosion from the most mountainous 10 % of Earth's surface [24] to the total rock mass of these 10 %, which at an average mountain height of 3000 m and a rock density of $2650\,\mathrm{kg\,m^{-3}}$ would equate to about $m = 4 \times 10^{20}\,\mathrm{kg}$. With half of the global denudation of $28\,\mathrm{Gt\,yr^{-1}}$ affecting this amount under present-day conditions, this leads to an estimate of $\xi_2 \approx 3.5 \times 10^{-8}\,\mathrm{yr^{-1}}$. Assuming that the system is in equilibrium under present-day conditions, it follows that $\xi_1 = \xi_2$.

Additionally, we increase W with a rate of $1 \times 10^{-8}\,\mathrm{yr}^{-1}$ during Snowball events to account for the effect of glacial flour on weatherability [27].

S1.3.3 Sediment flux and erosion

Sediment flux is dominated by physical erosion rather than chemical weathering [28]. We therefore need to determine erosion as a function of temperature and $p_{\mathrm{CO_2}}$ to use it as a proxy for sediment flux.

We choose to model erosion based on a power-law relationship with continent weathering:

$$E = W E_0 \left(\frac{F^*_{\mathrm{cw}}}{W} \right)^{\alpha_{\mathrm{E}}}. \tag{27}$$

Harrison finds that, among river basins on present-day Earth, erosion E scales exponentially with temperature [29], leading to a similar overall temperature dependence of erosion and continent weathering ($\alpha_{\mathrm{E}} \approx 1$). Gaillardet et al. find a power-law relationship between fluvial erosion and weathering rates on present-day Earth, indicating that erosion has a stronger temperature-dependence than weathering ($\alpha_{\mathrm{E}} \approx 1.5$). However, reconstructed sedimentation rates over the Phanerozoic do not show a correlation with reconstructed global temperatures at all ($\alpha_{\mathrm{E}} \approx 0$) (see Fig. 2).

While weathering decreases to very low values when the Earth system approaches a Snowball state, erosion likely does not decrease as much due to glacial erosion. This potentially explains why we do not observe a temperature dependence in erosion rates over the Phanerozoic. We therefore choose an intermediate value and assume that α_{E} lies in the interval $[0, 1]$.

In the first half of our analysis, in which we treat weatherability as a constant parameter, we choose $\alpha_{\mathrm{E}} = 1$ for simplicity. This allows us to use a scaled continent weathering flux F_{cw} as a proxy for sediment flux F_{s}. In the second half, where we let weatherability evolve dynamically, we use $\alpha_{\mathrm{E}} = 0.5$, but our results do not depend sensitively on this choice. Only for $\alpha_{\mathrm{E}} = 1$, some mathematical degeneracies appear in the weatherability model (see section S3).

S2 Steady-state solution of the carbon cycle

We tune C_{tot} to let pre-industrial weathering and outgassing be in equilibrium. To compute the outgassing flux from C_{tot}, we have to calculate how

C_m and C_p depend on C_tot when they are in equilibrium, since outgassing depends on C_m and C_p. Since the total amount of carbon is conserved, $C_\mathrm{tot} = \text{const.}$, two of the reservoirs already determine the entire dynamics of the system. Therefore, setting two of the reservoir derivatives equal to zero is sufficient to find the equilibrium of the carbon cycle.

First, there is the outgassing-weathering equilibrium, which results from setting the derivative of the atmosphere-ocean reservoir to zero, $dC_\mathrm{o+a}/dt = 0$:

$$\underbrace{fF_\mathrm{sub} + F_\mathrm{degas}}_{\text{Outgassing } F_\mathrm{out}} = \underbrace{\frac{F_\mathrm{cw}}{2} + F_\mathrm{sfw}}_{\text{Weathering } F_\mathrm{w}}. \tag{28}$$

It implies that due to the weathering thermostat, atmospheric CO_2 evolves in a way that causes weathering to exactly balance outgassing. Outgassing is composed of both arc volcanism fF_sub and ridge degassing F_degas, while weathering is the sum of continent and seafloor weathering.

Second, there is the regassing-outgassing equilibrium, which can be obtained by setting the mantle derivative to zero, $dC_\mathrm{m}/dt = 0$:

$$(1-f)F_\mathrm{sub} = F_\mathrm{degas}. \tag{29}$$

It implies that the carbon subducted into the mantle is compensated by carbon outgassing at ridges.

The regassing-outgassing equilibrium Eq. 29 can be used to obtain the ratio between the equilibrium plate and mantle reservoir sizes, $C_\mathrm{p,0}$ and $C_\mathrm{m,0}$. We first insert the subduction and degassing fluxes,

$$(1-f)F_\mathrm{sub} = F_\mathrm{degas} \tag{30}$$

$$(1-f)\alpha v_\mathrm{p} C_\mathrm{p,0} = \beta v_\mathrm{p} C_\mathrm{m,0}. \tag{31}$$

Here, the constants $\alpha := L/A_\mathrm{p}$ and $\beta := 2Ld_\mathrm{melt} f_\mathrm{d}/V_\mathrm{m}$ were introduced for convenience. Now, a relation between the equilibrium sizes of plate and mantle reservoir can be found directly:

$$C_\mathrm{m,0} = (1-f)\frac{\alpha}{\beta} C_\mathrm{p,0} \approx 30\, C_\mathrm{p,0}. \tag{32}$$

With this result, the total outgassing can be determined as a function not of the individual reservoirs C_m and C_p, but of their sum $C_\mathrm{m} + C_\mathrm{p}$:

$$\begin{aligned} F_\mathrm{out} &= f\alpha v_\mathrm{p} C_\mathrm{p} + \beta v_\mathrm{p} C_\mathrm{m}, \\ &= \frac{\alpha\beta}{(1-f)\alpha + \beta} v_\mathrm{p} (C_\mathrm{m} + C_\mathrm{p}) \end{aligned}$$

By defining another constant $\gamma := \frac{\alpha\beta}{(1-f)\alpha+\beta}$, this results in the outgassing flux under the condition that the mantle is in equilibrium

$$F_{\mathrm{out}}(C_{\mathrm{o+a}})\Big|_{dC_{\mathrm{m}}/dt=0} = \gamma v_{\mathrm{p}}(C_{\mathrm{tot}} - C_{\mathrm{o+a}}). \tag{33}$$

In the last step, the sum of the mantle and plate reservoirs $C_{\mathrm{m}} + C_{\mathrm{p}}$, has been replaced by the total amount of carbon minus the carbon in atmosphere and ocean $C_{\mathrm{tot}} - C_{\mathrm{o+a}}$. Similarly to the individual subduction and degassing fluxes, the total outgassing scales linearly with plate velocity v_{p} and the combined amount of carbon in plate and mantle, $C_{\mathrm{m}} + C_{\mathrm{p}}$.

Therefore, for fixed C_{tot}, the outgassing at regassing-degassing equilibrium has been found as a function of $C_{\mathrm{o+a}}$:

$$F_{\mathrm{w}}(C_{\mathrm{o+a}}) = F_{\mathrm{out}}(C_{\mathrm{o+a}})\Big|_{dC_{\mathrm{m}}/dt=0}. \tag{34}$$

To obtain the steady state solution of the carbon cycle, one has to solve this equation for $C_{\mathrm{o+a}}$. The remaining carbon $C_{\mathrm{tot}} - C_{\mathrm{o+a}}$ is then partitioned between C_{m} and C_{p} according to equation 32.

We start by noting that, in order to obtain a weathering flux on the order of its pre-industrial value, the atmosphere-ocean reservoir must have a size of approximately $C_{\mathrm{o+a}} \approx 1 \times 10^{18}\,\mathrm{mol}$. To get a matching outgassing flux, the total amount of carbon according to Eq. 34 must be on the order of $C_{\mathrm{tot}} \approx 1 \times 10^{22}\,\mathrm{mol}$. Therefore, only a negligible fraction of total carbon resides in the atmosphere and ocean reservoir, allowing to simplify equation 34 to

$$F_{\mathrm{out}}(C_{\mathrm{o+a}})\Big|_{dC_{\mathrm{m}}/dt=0} = \gamma v_{\mathrm{p}}(C_{\mathrm{tot}} - C_{\mathrm{o+a}}) \approx \gamma v_{\mathrm{p}} C_{\mathrm{tot}} \tag{35}$$

Now, by equating the outgassing flux F_{out} with the present-day weathering flux $F_{\mathrm{w,0}}$, the total amount of carbon can be obtained,

$$C_{\mathrm{tot}} = \frac{F_{\mathrm{w,0}}}{v_{\mathrm{p}}\gamma} \approx 2.26 \times 10^{22}\,\mathrm{mol}. \tag{36}$$

The value found in this way agrees well with the value used by Foley, $C_{\mathrm{tot}} = 2.5 \times 10^{22}\,\mathrm{mol}$ [9].

To actually solve the steady state of the carbon cycle, equation 35 can be solved graphically or numerically. In the main paper, we make use of the fact that plate velocity is a function of sediment flux, which we determine from continent weathering: $v_\mathrm{p} = v_\mathrm{p}(F_\mathrm{s}) = v_\mathrm{p}(F_\mathrm{cw})$. We also express total weathering F_w as a function of continent weathering F_cw, which is only possible numerically, since to this end, the seafloor weathering flux F_sfw has to be inverted and given as a function of F_cw. However, since $F_\mathrm{cw} \gg F_\mathrm{sfw}$, weathering is almost identical to continent weathering, resulting in an almost linear relationship: $F_\mathrm{w}(F_\mathrm{cw}) \approx F_\mathrm{cw}$.

$$F_\mathrm{cw} \approx \gamma v_\mathrm{p}(F_\mathrm{cw}) C_\mathrm{tot}. \tag{37}$$

This equation can then be solved graphically to determine F_cw and v_p at outgassing-weathering equilibrium, which we have done in main figure 3.

S3 Weatherability steady states

As described in the main paper, the dynamic evolution of weatherability according to Eq. 26 leads to a second positive feedback: An increase in plate velocity leads to an increase in weatherability. Thus, erosion is enhanced, leading to an increase in sediment flux and therefore a further increase in plate velocity.

This feedback also leads to the existence of two stable states at low and high plate velocity respectively. The states are determined by the intersections of the sigmoid curve $\xi_1 v_\mathrm{p}(E)$ and the linear function $\xi_2 E^*$, again giving rise to three intersections corresponding to two stable and one unstable state (see Fig. 3). One of the steady states is again determined by low plate velocity $v_\mathrm{p} \approx v_\mathrm{p,min}$ and low erosion $E \approx 0.2\, E_0$, while the other one is determined by high plate velocity $v_\mathrm{p} \approx v_\mathrm{p,max}$ and high erosion $E \approx E_0$.

These states of steady weatherability are generally compatible with the outgassing-weathering equilibrium and therefore correspond to steady states of the entire model. To see this, we start by quantifying the condition of steady weatherability. By letting $dW/dt = 0$, equation 26 turns into $v_\mathrm{p}^* = E^*$. By writing erosion as $E^* = W f_\mathrm{E}(T, p_{\mathrm{CO}_2})$, where f_E incorporates the climate dependence of erosion, we arrive at

$$v_\mathrm{p}^* = W f_\mathrm{E}(T, p_{\mathrm{CO}_2}). \tag{38}$$

Weatherability is in steady state when it satisfies this equation.

The outgassing-weathering equilibrium is given by

$$F_\mathrm{w}^* = v_\mathrm{p}^*. \tag{39}$$

We expand the weathering flux into continent and seafloor weathering:

$$v_{\mathrm{p}}^{*} = F_{\mathrm{cw}}^{*} + F_{\mathrm{sfw}}^{*} \tag{40}$$

$$= W f_{\mathrm{cw}}(T, p_{\mathrm{CO_2}}) + v_{\mathrm{p}}^{*} f_{\mathrm{sfw}}(T, p_{\mathrm{CO_2}}). \tag{41}$$

Here, the functions f_i again denote the climate dependence of the weathering fluxes. We can now insert this equation into Eq. 38:

$$W f_{\mathrm{E}}(T, p_{\mathrm{CO_2}}) = W f_{\mathrm{cw}}(T, p_{\mathrm{CO_2}}) + v_{\mathrm{p}}^{*} f_{\mathrm{sfw}}(T, p_{\mathrm{CO_2}}). \tag{42}$$

This equation needs to be fulfilled if the states of steady weatherability are also steady states of the whole model. By solving Eq. 41 for W and substituting it into Eq. 42, we arrive at:

$$f_{\mathrm{E}} - f_{\mathrm{cw}} = f_{\mathrm{E}} f_{\mathrm{sfw}}. \tag{43}$$

Remarkably, this equation is independent of v_{p}. Therefore, if a solution to it exists (i.e., if there is a climate state for which the whole model is in equilibrium), the equilibrium climate is the same for both tectonic states. This is due to the fact that the effects of outgassing and weatherability on climate counteract and cancel out exactly in our model. In the next section, we discuss the effect of outgassing sources independent of plate velocity on this balance.

Under preindustrial conditions, by definition $f_{\mathrm{E}} = 1$ and $f_{\mathrm{cw}} + f_{\mathrm{sfw}} = 1$, so Eq. 43 is fulfilled for any erosion or weathering parametrization. At lower solar luminosities, pre-industrial CO_2 leads to lower temperatures than pre-industrial T_0. As a consequence, Eq. 43 is not fulfilled for pre-industrial CO_2 in the deep past.

Since $f_{\mathrm{sfw}} \ll f_{\mathrm{cw}}$, solving Eq. 43 essentially means finding an intersection between f_{E} and f_{cw}. At low temperatures close to a Snowball state, weathering is likely low due to the diminished hydrological cycle, while erosion is relatively high due to glacial erosion, so we should expect that $f_{\mathrm{E}} > f_{\mathrm{cw}}$. On the other hand, at high temperatures, there is likely an upper limit to precipitation [30], which should also lead to an upper limit to erosion, while the rate of chemical weathering reactions still increases with temperature until weathering enters the supply-limited regime determined by the rate of exposure of unweathered rock through erosion [31]: $f_{\mathrm{E}} < f_{\mathrm{cw}}$. As a consequence, we should expect an intersection between the two curves somewhere in the Greenhouse regime, and therefore also a steady state of the whole system according to Eq. 43, regardless of the exact weathering or erosion formulation. However, the exact position of the intersection – and therefore, the climate state – of course depends sensitively on the parametrizations. Therefore, while the bistable properties of the model are robust to changes in parameters, temperature is not.

We note that our model exhibits a mathematical degeneracy when the erosion and continent weathering parametrizations are identical, i.e., $\alpha_{\mathrm{E}} = 1$. This can be seen from Eq. 42, which, for $f_{\mathrm{cw}} = f_{\mathrm{E}}$, turns into

$$0 = v_{\mathrm{p}}^* f_{\mathrm{sfw}}(T, p_{\mathrm{CO_2}}). \tag{44}$$

This equation is not solvable since $v_{\mathrm{p}} \neq 0$ and $f_{\mathrm{sfw}}(T, p_{\mathrm{CO_2}}) \neq 0$. As a consequence, there are no steady states of the whole model. This can be explained using Eq. 26:

$$\frac{dW^*}{dt} = \xi_1 v_{\mathrm{p}}^* - \xi_2 E^*(W). \tag{45}$$

If erosion and continent weathering have the same climate dependence, we can exchange E^* with F_{cw}^*,

$$\frac{dW^*}{dt} \approx \xi_1 v_{\mathrm{p}}^* - \xi_2 F_{\mathrm{cw}}^*. \tag{46}$$

Due to the weathering thermostat, weathering is essentially determined by outgassing, $F_{\mathrm{cw}}/2 + F_{\mathrm{sfw}} = F_{\mathrm{out}}$, so we can write approximately

$$\frac{dW^*}{dt} \approx \xi_1 v_{\mathrm{p}}^* - \xi_2 \left(F_{\mathrm{out}}^* - \frac{F_{\mathrm{sfw}}}{F_{\mathrm{out},0}} \right). \tag{47}$$

Since outgassing is proportional to plate velocity, $F_{\mathrm{out}}^* = v_{\mathrm{p}}^*$ and $\xi_1 = \xi_2$, this reduces to

$$\frac{dW^*}{dt} = \xi_2 \frac{F_{\mathrm{sfw}}}{F_{\mathrm{out},0}} > 0. \tag{48}$$

As a consequence, there is a run-away weatherability for $\alpha_{\mathrm{E}} = 1$. In the future, this model instability could be resolved by differentiating between weatherability and global erodibility.

S4 Climate influence of plate-velocity-independent degassing

If we assume that there is a contribution to outgassing that is not proportional to plate velocity (e.g., plume or LIP volcanism), there is a difference between the climate of the slow and the fast state. We modify the degassing flux to contain a second term independent of plate velocity (Eq. 13):

$$F_{\mathrm{degas}} = \zeta f_{\mathrm{d}} \frac{C_{\mathrm{m}}}{V_{\mathrm{m}}} 2 L d_{\mathrm{melt}} v_{\mathrm{p}} + (1-\zeta) H C_{\mathrm{m}}. \tag{49}$$

To analyze the effect of non-zero hotspot outgassing, we need to convert from the ratio of plate-velocity dependent degassing to total mantle degassing ζ to the ratio of plate-velocity dependent outgassing to total outgassing (including arc volcanism) $\hat{\zeta}$.

At equilibrium, mantle degassing and regassing are balanced:

$$F_{\mathrm{degas}} = (1-f) F_{\mathrm{sub}}. \tag{50}$$

$(1-\zeta)$ is defined as the ratio of hotspot degassing F_{H} to total mantle degassing:

$$1-\zeta = \frac{F_{\mathrm{H}}}{F_{\mathrm{degas}}} = \frac{F_{\mathrm{H}}}{(1-f) F_{\mathrm{sub}}}. \tag{51}$$

$(1-\hat{\zeta})$ is defined as the ratio of hotspot degassing to total outgassing, including arc volcanism $f F_{\mathrm{sub}}$,

$$1-\hat{\zeta} = \frac{F_{\mathrm{H}}}{F_{\mathrm{degas}} + f F_{\mathrm{sub}}} = \frac{F_{\mathrm{H}}}{F_{\mathrm{sub}}}. \tag{52}$$

As a consequence, we can convert from ζ to $\hat{\zeta}$ as follows:

$$1-\hat{\zeta} = (1-\zeta)(1-f). \tag{53}$$

It should be noted that for $\zeta \neq 1$, the equilibrium ratio between C_{m} and C_{p} depends slightly on v_{p}. This also affects the total outgassing flux F_{out}, leading to increased outgassing in the slow state. The following calculation is therefore only a first-order approximation, resulting in a lower bound to the temperature difference between the two states.

Using $\hat{\zeta}$, we can now calculate total outgassing:

$$F^*_{\text{out}} = \hat{\zeta} v^*_{\text{p}} + (1 - \hat{\zeta}), \tag{54}$$

which leads to a change to the outgassing-weathering equilibrium:

$$\hat{\zeta} v^*_{\text{p}} + (1 - \hat{\zeta}) = W f_{\text{cw}}(T, p_{\text{CO}_2}) + v^*_{\text{p}} f_{\text{sfw}}(T, p_{\text{CO}_2}). \tag{55}$$

We again insert Eq. 38 and eliminate W, which results in

$$v^*_{\text{p}} f_{\text{E}} f_{\text{sfw}} + v^*_{\text{p}} f_{\text{cw}} = \hat{\zeta} v^*_{\text{p}} f_{\text{E}} + (1 - \hat{\zeta}) f_{\text{E}} \tag{56}$$

For $\hat{\zeta} = 1$, this reduces to Eq. 43. For the fast state, $v^*_{\text{p}} = 1$, the equation also becomes identical to Eq. 43, meaning that the climate of the fast state remains unaffected by this modification.

Using the definition of erosion,

$$f_{\text{E}} = f_{\text{cw}}^{\alpha_{\text{E}}}, \tag{57}$$

we can write:

$$f_{\text{cw}}^{1-\alpha_{\text{E}}} + f_{\text{sfw}} = \frac{1 - \hat{\zeta}}{v^*_{\text{p}}} + \hat{\zeta}. \tag{58}$$

Bearing in mind that $F_{\text{sfw}} \ll F_{\text{cw}}$, this shows that – as long as α_{E} is in the interval $[0, 1]$ – f_{cw} increases when v^*_{p} is decreased. The closer α_{E} is to 1, the more pronounced the effect gets, until it diverges at $\alpha_{\text{E}} = 1$, which is due to the general model degeneracy at that point.

We therefore use $\alpha_{\text{E}} = 0$ to quantify the minimum effect of hotspot outgassing on climate. We neglect cases where α_{E} is either below 0 (meaning erosion would decrease when weathering increases) or above 1. We use the outgassing fluxes reported by Marty and Tolstikhin [32] to estimate $\hat{\zeta}$. Since only an upper limit to hotspot outgassing is reported, we use half of that value as a best guess estimate, resulting in $\hat{\zeta} = 0.75$ (equivalent to $\zeta = 0.5$, which we use in the 2.75 Ga model integration). We then use a Monte-Carlo approach to propagate the uncertainty in the weathering function to our estimate of the slow state climate. For the dependence of continent weathering on p_{CO_2}, we use the error range reported by [10]. For the temperature dependence, we use a median value of 10 K, and a 68 % confidence interval of [5 K to 45 K], according to the minimum estimates in literature [6] and upper end of the confidence interval in [10].

S5 Sediment buoyancy effect

There is evidence that very high sediment fluxes can actually lead to diminished plate velocities, because sedimentary rock typically has a lower density than oceanic crust and therefore increases the buoyancy of the subducted plate [33, 34]. Therefore, we test an alternative plate velocity parametrization, which incorporates a reduction of plate velocities at high sediment flux by multiplying the original plate velocity parametrization by another tanh-function:

$$\begin{aligned} v_{\mathrm{p}}(F_{\mathrm{cw}}) = v_{\mathrm{min}} + \frac{1}{4}\Big(v_{\mathrm{max}} - v_{\mathrm{min}}\Big)\Big(1 + \tanh s_{\mathrm{p}}(F_{\mathrm{s}} - F_{\mathrm{S,ref}})\Big) \\ \Big(1 - \tanh s_{\mathrm{p}}(F_{\mathrm{s}} - F_{\mathrm{S,ref2}})\Big). \end{aligned} \tag{59}$$

For simplicity, we set the second transition point – at which the transition from fast to slow plate velocities due to sediment buoyancy – to twice the value of the first transition from slow to fast, $F_{\mathrm{cw,ref2}} = 2\,F_{\mathrm{cw,ref}}$.

Analogously to the original model setup, the steady states of the system can be determined by examining the intersections between the actual plate velocity $v_{\mathrm{p}}(F_{\mathrm{cw}})$ and the plate velocity determined by the outgassing-weathering equilibrium $v_{\mathrm{p}}^{\mathrm{owe}}(F_{\mathrm{cw}})$. As can be seen from figure 4, the steady states are not affected by the alternative plate velocity parametrization. Only if the sediment buoyancy effect occurred at similar values as the sediment lubrication effect, $F_{\mathrm{cw,ref2}} \approx F_{\mathrm{cw,ref}}$, the long-term behaviour of the model would be affected. This would however invalidate the entire sediment-lubrication hypothesis, since no significant increase in plate velocity due to sediment subduction would be possible under such circumstances.

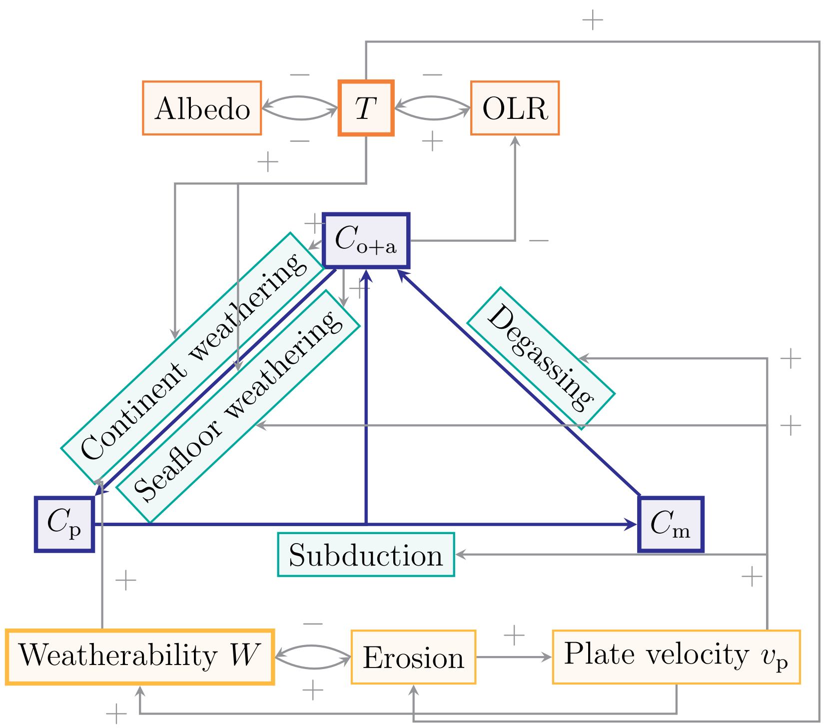

Figure 1: Full model overview. Grey arrows indicate positive or negative relationship. Blue arrows indicate carbon fluxes. Bold box contours indicate that a variable is a state variable.

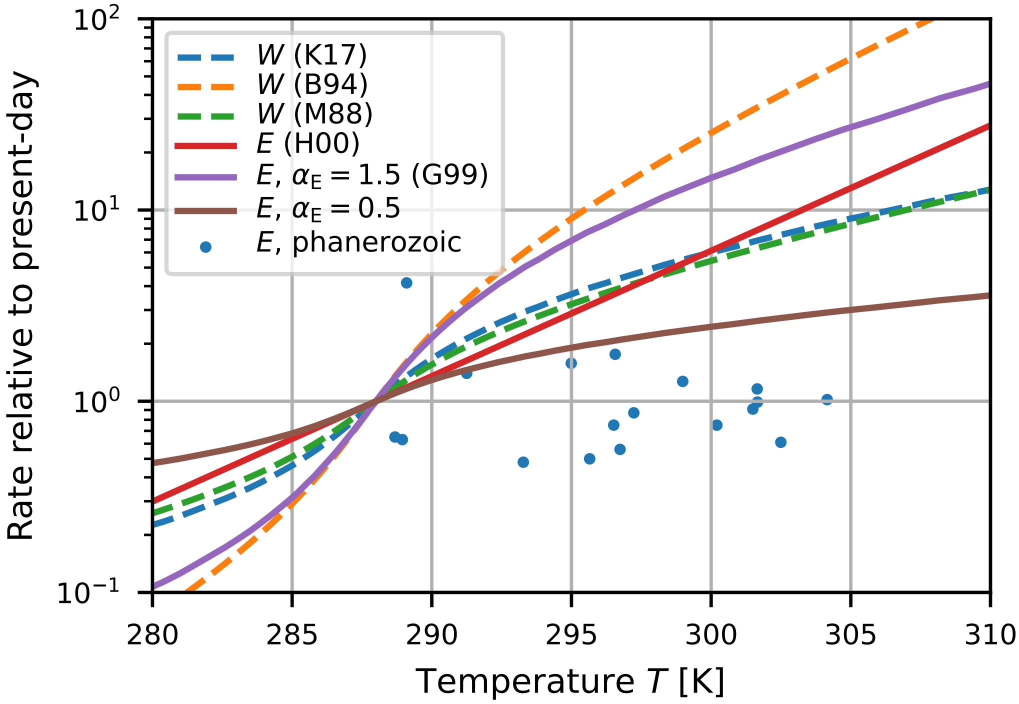

Figure 2: Temperature dependence of erosion (E) and weathering (W) according to several published parametrizations. K17: Krissansen-Totton and Catling [10], B94: Berner [11], M88: Marshall et al. [13], H00: Harrison [29]. G99: Gaillardet et al. [28], also see eq. 9 in [35]. Power-law dependence of erosion on weathering found in present-day data. Based here on K17 weathering. E, $\alpha_{\mathrm{E}} = 0.5$: Parametrization used for the second part of our analysis. E, phanerozoic: Erosion rates over the Phanerozoic [35] plotted against reconstructed global sea-surface temperature [36]. Shaded regions indicate the confidence intervals (light color: 90 %, darker color: 68 %) if given in original parametrization.

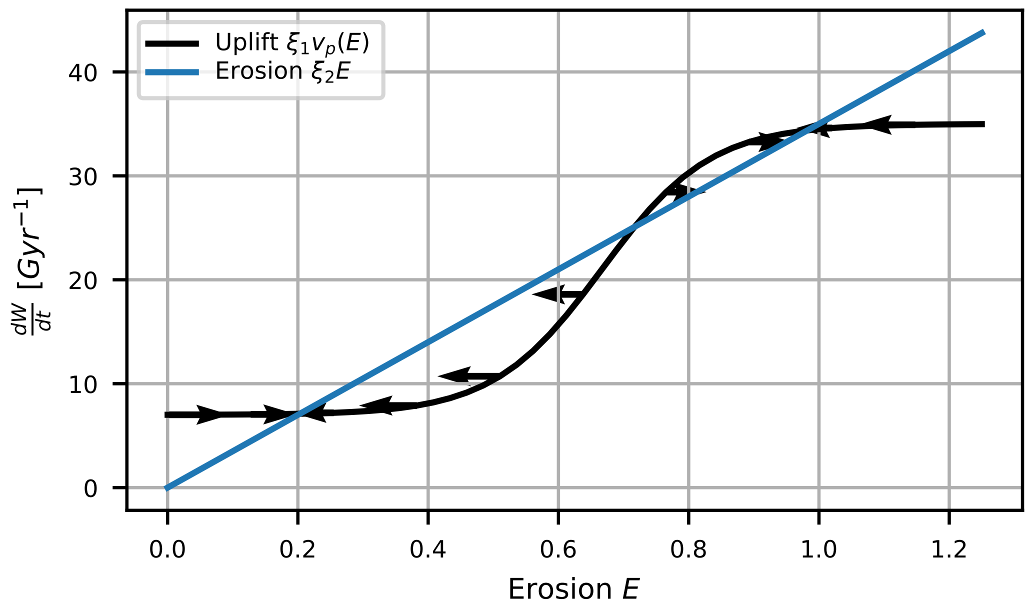

Figure 3: States of steady weatherability. Changes in weatherability W are determined by uplift $\xi_1 v_\mathrm{p}(E)$ and erosion $\xi_2 E$, both of which are functions of E. When the contributions from uplift and erosion are identical, the time derivative of weatherability is zero, $dW/dt = 0$. Therefore, steady states are determined by intersections between the two curves. Analogously to the outgassing-weathering equilibrium, there are three intersections, corresponding to three steady states. However, only the intersections at low and high plate velocity correspond to stable states, since the intermediate steady state is unstable, as can be seen from the black arrows.

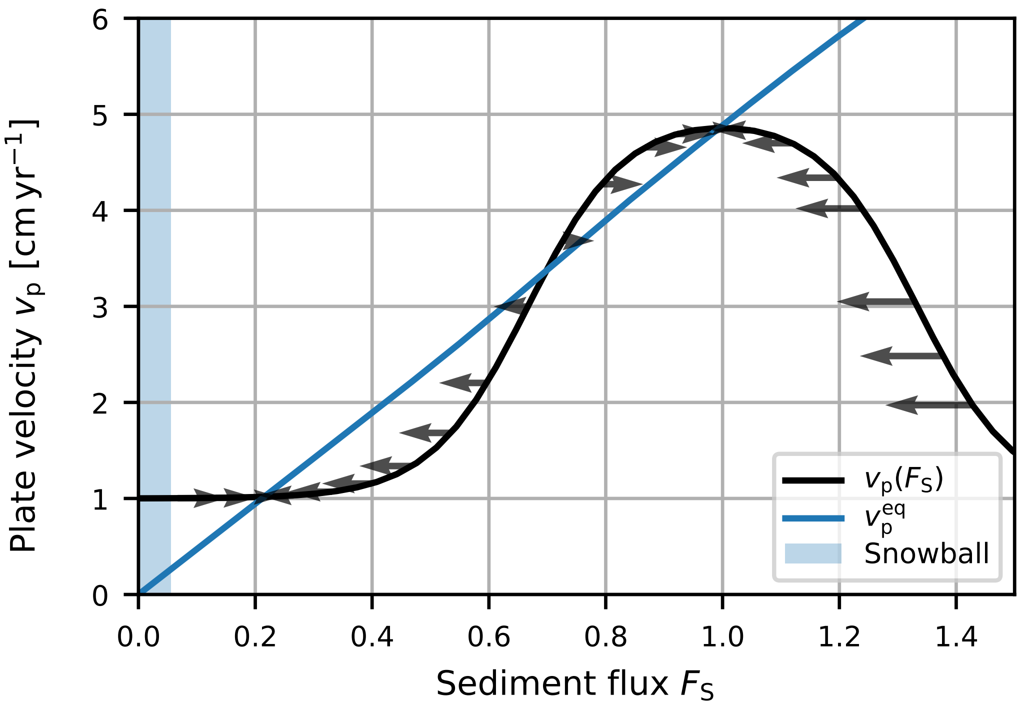

Figure 4: Outgassing-weathering equilibrium for an alternative plate velocity parametrization. High sediment thickness potentially leads to reduced plate velocities [37]. As long as a significant peak in plate velocity remains, this does not alter the number or position of intersections between the outgassing-weathering equilibrium condition (blue) and the actual plate velocity (black). Therefore, the long-term model behaviour remains unaffected.

Variable	**Description**	**Type**	**Units**	**Equation**
T	Global surface temperature	Diagnostic	K	Eq. 1
OLR	Outgoing long-wave radiation	Diagnostic	$\mathrm{W\,m^{-2}}$	Eq. 2
ASR	Absorbed solar radiation	Diagnostic	$\mathrm{W\,m^{-2}}$	Eq. 3
S	Solar luminosity	Diagnostic	$\mathrm{W\,m^{-2}}$	Eq. 4
α	Planetary albedo	Diagnostic	[]	Eq. 5

Table 1: Model variables – climate model

Parameter	**Description**	**Value**	**Source**
T_0	Pre-industrial temperature	288 K	[38]
$p_{\mathrm{CO_2},0}$	Pre-industrial partial pressure of CO_2	30 Pa	[38]
a_{OLR}	Slope of OLR with temperature	$2\,\mathrm{W\,m^{-2}\,K^{-1}}$	[38]
b_{OLR}	Slope of OLR with the logarithm of $p_{\mathrm{CO_2}}$	$10\,\mathrm{W\,m^{-2}}$	[38]
S_0	Present day solar flux	$1364\,\mathrm{W\,m^{-2}}$	[38]
α_{ice}	Planetary albedo of Snowball Earth	0.6	[5, 38]
$\alpha_{\mathrm{no-ice}}$	Planetary albedo of ice-free Earth	0.3	[5, 38]
γ_{albedo}	Smoothness of albedo step function	0.7	Derived
T_{ref}	Snowball transition temperature	267.5 K	Derived
$t_{\odot}$	Age of the sun	4.7 Gyr	[3]

Table 2: Model parameters – climate

Variable	Description	Type	Units	Equation
C_{p}	Carbon reservoir oceanic plates	Prognostic	mol	Eq. 6
C_{m}	Carbon reservoir mantle	Prognostic	mol	Eq. 6
$C_{\mathrm{o+a}}$	Carbon reservoir atmosphere and ocean	Prognostic	mol	Eq. 6
F_{cw}	Continent weathering	Diagnostic	$\mathrm{mol\,yr^{-1}}$	Eq. 14
F_{sfw}	Seafloor weathering	Diagnostic	$\mathrm{mol\,yr^{-1}}$	Eq. 15
F_{sub}	Carbon subduction	Diagnostic	$\mathrm{mol\,yr^{-1}}$	Eq. 12
F_{degas}	Mantle carbon degassing	Diagnostic	$\mathrm{mol\,yr^{-1}}$	Eq. 11
F_{w}	Total weathering	Diagnostic	$\mathrm{mol\,yr^{-1}}$	Eq. 9
F_{out}	Total carbon outgassing	Diagnostic	$\mathrm{mol\,yr^{-1}}$	Eq. 10
$p_{\mathrm{CO_2}}$	Partial pressure of CO_2	Diagnostic	Pa	Eq. 20
$[H^+]$	Hydrogen molarity of seawater	Diagnostic	[]	Eq. 23

Table 3: Model variables – carbon cycle model

Parameter	Description	Value	Source
f	Fraction of subducted carbon that degasses	0.5	[9]
f_d	Fraction of upwelling mantle that degasses	0.32	[9]
V_m	Volume of the mantle	$9.1 \times 10^{20}\,\mathrm{m}^3$	[9]
L	Total trench length	$6 \times 10^{7}\,\mathrm{m}$	[9]
d_melt	Depth of melting beneath ridges	$7 \times 10^{4}\,\mathrm{m}$	[9]
H	Hotspot outgassing constant	$2 f_\mathrm{d} L d_\mathrm{melt} v_{\mathrm{p},0}/V_\mathrm{m}$	derived
f_land	Present-day land fraction	0.3	[9]
A_Earth	Earth surface area	$5.1 \times 10^{14}\,\mathrm{m}^2$	[9]
A_p	Area of oceanic plates	$(1 - f_\mathrm{land}) A_\mathrm{Earth}$	derived
$F_{\mathrm{cw},0}$	Present-day continent weathering flux	$12 \times 10^{12}\,\mathrm{mol\,yr^{-1}}$	[28]
χ_cc	Fraction of weatherable ions in crust	0.08	[9]
m_cc	Molar mass of weatherable ions	$32\,\mathrm{g\,mol^{-1}}$	[9]
a_cw	$p_{\mathrm{CO_2}}$ exponent for continent weathering	0.33	[10]
T_cw	e-folding temperature for continent weathering	$10\,\mathrm{K}$	[6]
$F_{\mathrm{sfw},0}$	Present-day seafloor weathering flux	$4.5 \times 10^{11}\,\mathrm{mol\,yr^{-1}}$	[10]
k_diss	Seafloor weathering prefactor	$2.23 \times 10^{25}\,\mathrm{mol\,yr^{-1}}$	Section S1.2.3
γ_sfw	Seafloor weathering hydrogen molarity exponent	0.27	[10]
$v_{\mathrm{p},0}$	Present-day plate velocity	$0.05\,\mathrm{m\,yr^{-1}}$	[9]
E_bas	Basalt dissolution activation energy	$75\,000\,\mathrm{J\,mol^{-1}}$	[15]
R	Universal gas constant	$8.314\,\mathrm{J\,K^{-1}\,mol^{-1}}$	
$c_\mathrm{deep-water}$	Slope of deep water temperature with T	1.02	[10]
$b_\mathrm{deep-water}$	y-axis intercept of deep-water temperature	$-16.7\,\mathrm{K}$	[10]

b_{pore}	Heating of deep water in oceanic crust	$9\,\mathrm{K}$	[39]
b_{pH}	pH y-axis intercept	12.2	Section S1.2.4
c_{pH}	Slope of logarithmic $p_{\mathrm{CO_2}}$ with pH	1.9	Section S1.2.4
$\alpha_{\mathrm{H_2O}}$	Activity coefficient in Eq. 19	$0.967\,\mathrm{mol\,L^{-1}}$	[17]
$\gamma_{\mathrm{H_2CO_3}}$	Activity coefficient in Eq. 19	1.130	[17]
$\gamma_{\mathrm{HCO_3{}^-}}$	Activity coefficient in Eq. 19	0.550	[17]
$\gamma_{\mathrm{CO_3{}^{2-}}}$	Activity coefficient in Eq. 19	0.021	[17]
K_0	Equilibrium constant in Eq. 19	$3.48 \times 10^{-7}\,\mathrm{Pa^{-1}}$	[17]
K_1	Equilibrium constant in Eq. 19	$4.45 \times 10^{-7}\,\mathrm{mol\,L^{-1}}$	[17]
K_2	Equilibrium constant in Eq. 19	$4.69 \times 10^{-11}\,\mathrm{mol\,L^{-1}}$	[17]
g	Gravitational acceleration	$9.8\,\mathrm{m\,s^{-2}}$	[17]
C_{tot}	Total carbon amount	$2.26 \times 10^{22}\,\mathrm{mol}$	Section S2

Table 4: Model parameters – carbon cycle

Variable	Description	Type	Units	Equation
W	Weatherability	Prognostic	[]	Eq. 26
v_p	Plate velocity	Diagnostic	$\mathrm{cm\,yr^{-1}}$	Eq. 24
F_s	Sediment flux	Diagnostic	$\mathrm{mol\,yr^{-1}}$	Sec. S1.3.3
E	Erosion	Diagnostic	$\mathrm{mol\,yr^{-1}}$	Eq. 27

Table 5: Model variables – geodynamics model

Parameter	Description	Value	Source
ξ_1	Slope of weatherability production proportional to v_p	$3.5\times10^{-8}\,\mathrm{yr^{-1}}$	Section S1.3.2
ξ_2	Slope of W reduction proportional to W	$3.5\times10^{-8}\,\mathrm{yr^{-1}}$	Section S1.3.2
v_min	Minimum plate velocity	$v_\mathrm{p,0}/5$	Eq. 24
v_max	Maximum plate velocity	$v_\mathrm{p,0}$	Eq. 24
$F_\mathrm{S,ref}$	Reference continent weathering flux	$2/3\,F_\mathrm{S,0}$	Eq. 24
s_p	Steepness of sigmoid plate velocity curve	$4/F_\mathrm{cw,0}$	Eq. 24
α_E	Continent weathering exponent for erosion	1, 0.5	Section S1.3.3

Table 6: Model parameters – geodynamics

References

[1] J. C. G. Walker, P. B. Hays, and J. F. Kasting, "A negative feedback mechanism for the long-term stabilization of Earth's surface temperature", Journal of Geophysical Research: Oceans **86**, 9776–9782 (1981).

[2] D. M. Williams and J. F. Kasting, "Habitable Planets with High Obliquities", Icarus **129**, 254–267 (1997).

[3] D. O. Gough, "Solar Interior Structure and Luminosity Variations", Solar Physics **74**, 21–34 (1981).

[4] G. R. North and K.-Y. Kim, *Energy Balance Climate Models* (John Wiley & Sons, Dec. 2017).

[5] B. Mills, A. J. Watson, C. Goldblatt, et al., “Timing of Neoproterozoic glaciations linked to transport-limited global weathering”, Nature Geoscience **4**, 861–864 (2011).

[6] D. S. Abbot, N. B. Cowan, and F. J. Ciesla, “Indication of Insensitivity of Planetary Weathering Behavior and Habitable Zone to Surface Land Fraction”, The Astrophysical Journal **756**, 178 (2012).

[7] G. Feulner, M. Bukenberger, and S. Petri, “Tracing the Snowball bifurcation of aquaplanets through time reveals a fundamental shift in critical-state dynamics”, Earth System Dynamics **14**, 533–547 (2023).

[8] J. Wu, Y. Liu, and Z. Zhao, “How Should Snowball Earth Deglaciation Start”, Journal of Geophysical Research: Atmospheres **126**, e2020JD033833 (2021).

[9] B. J. Foley, “The Role of Plate Tectonic–Climate Coupling and Exposed Land Area in the Development of Habitable Climates on Rocky Planets”, The Astrophysical Journal **812**, 36 (2015).

[10] J. Krissansen-Totton and D. C. Catling, “Constraining climate sensitivity and continental versus seafloor weathering using an inverse geological carbon cycle model”, Nature Communications **8**, 15423 (2017).

[11] R. A. Berner, “GEOCARB II; a revised model of atmospheric CO 2 over Phanerozoic time”, American Journal of Science **294**, 10.2475/ajs.294.1.56 (1994).

[12] D. S. Abbot, A. Voigt, M. Branson, et al., “Clouds and Snowball Earth deglaciation”, Geophysical Research Letters **39**, 10.1029/2012GL052861 (2012).

[13] H. G. Marshall, J. C. G. Walker, and W. R. Kuhn, “Long-term climate change and the geochemical cycle of carbon”, Journal of Geophysical Research: Atmospheres **93**, 791–801 (1988).

[14] B. P. C. Hayworth and B. J. Foley, “Waterworlds May Have Better Climate Buffering Capacities than Their Continental Counterparts”, The Astrophysical Journal Letters **902**, L10 (2020).

[15] J. Krissansen-Totton, G. N. Arney, and D. C. Catling, “Constraining the climate and ocean pH of the early Earth with a geological carbon cycle model”, Proceedings of the National Academy of Sciences **115**, 4105–4110 (2018).

[16] J. Chambers, "The Effect of Seafloor Weathering on Planetary Habitability", The Astrophysical Journal **896**, 96 (2020).

[17] S. Franck, K. J. Kossacki, W. Von Bloh, et al., "Long-term evolution of the global carbon cycle: historic minimum of global surface temperature at present", Tellus B **54**, 325–343 (2002).

[18] S. Lamb and P. Davis, "Cenozoic climate change as a possible cause for the rise of the Andes", Nature **425**, 792–797 (2003).

[19] J. Li, D. J. Shillington, D. M. Saffer, et al., "Connections between subducted sediment, pore-fluid pressure, and earthquake behavior along the Alaska megathrust", Geology **46**, 299–302 (2018).

[20] H. Zhou, J. Hu, L. Dal Zilio, et al., "India–Eurasia convergence speed-up by passive-margin sediment subduction", Nature **635**, 114–120 (2024).

[21] A. E. Pusok, D. R. Stegman, and M. Kerr, "The effect of low-viscosity sediments on the dynamics and accretionary style of subduction margins", Solid Earth **13**, 1455–1473 (2022).

[22] C. Liu, R. X. Shi, Y. H. Zhang, et al., "2015: How Many Islands (Isles, Rocks), How Large Land Areas and How Long of Shorelines in the World? ——Vector Data based on Google Earth Images", Journal of Global Change Data & Discovery **3**, 124–148 (2019).

[23] J. Syvitski, J. R. Ángel, Y. Saito, et al., "Earth's sediment cycle during the Anthropocene", Nature Reviews Earth & Environment **3**, 179–196 (2022).

[24] I. J. Larsen, D. R. Montgomery, and H. M. Greenberg, "The contribution of mountains to global denudation", Geology **42**, 527–530 (2014).

[25] D. Höning and T. Spohn, "Land Fraction Diversity on Earth-like Planets and Implications for Their Habitability", Astrobiology **23**, 372–394 (2023).

[26] D. Höning and T. Spohn, "Continental growth and mantle hydration as intertwined feedback cycles in the thermal evolution of Earth", Physics of the Earth and Planetary Interiors **255**, 27–49 (2016).

[27] S. Fabre and G. Berger, "How tillite weathering during the snowball Earth aftermath induced cap carbonate deposition", Geology **40**, 1027–1030 (2012).

[28] J. Gaillardet, B. Dupre, P. Louvat, et al., "Global silicate weathering and CO2 consumption rates deduced from the chemistry of large rivers", Chemical Geology **159**, 3–30 (1999).

[29] C. G. A. Harrison, "What factors control mechanical erosion rates?", International Journal of Earth Sciences **88**, 752–763 (2000).

[30] P. A. O'Gorman and T. Schneider, "The Hydrological Cycle over a Wide Range of Climates Simulated with an Idealized GCM", Journal of Climate **21**, 3815–3832 (2008).

[31] E. J. Gabet and S. M. Mudd, "A theoretical model coupling chemical weathering rates with denudation rates", Geology **37**, 151–154 (2009).

[32] B. Marty and I. N. Tolstikhin, "CO2 fluxes from mid-ocean ridges, arcs and plumes", Chemical Geology **145**, 233–248 (1998).

[33] S. Brizzi, T. W. Becker, C. Faccenna, et al., "The Role of Sediment Accretion and Buoyancy on Subduction Dynamics and Geometry", Geophysical Research Letters **48**, e2021GL096266 (2021).

[34] W. M. Behr, A. F. Holt, T. W. Becker, et al., "The effects of plate interface rheology on subduction kinematics and dynamics", Geophysical Journal International **230**, 796–812 (2022).

[35] R. A. Berner, "GEOCARB III: A revised model of atmospheric CO2 over Phanerozoic time", American Journal of Science **301**, 182–204 (2001).

[36] E. J. Judd, J. E. Tierney, D. J. Lunt, et al., "A 485-million-year history of Earth's surface temperature", Science **385**, eadk3705 (2024).

[37] S. Brizzi, I. van Zelst, F. Funiciello, et al., "How Sediment Thickness Influences Subduction Dynamics and Seismicity", Journal of Geophysical Research: Solid Earth **125**, e2019JB018964 (2020).

[38] D. S. Abbot, "Analytical Investigation of the Decrease in the Size of the Habitable Zone Due to a Limited CO_2 Outgassing Rate", The Astrophysical Journal **827**, 117 (2016).

[39] L. A. Coogan and S. E. Dosso, "Alteration of ocean crust provides a strong temperature dependent feedback on the geological carbon cycle and is a primary driver of the Sr-isotopic composition of seawater", Earth and Planetary Science Letters **415**, 38–46 (2015).